Visual Servoing for Underactuated VTOL UAVs: a Linear, Homography-Based Approach

Henry de Plinval, Pascal Morin, Philippe Mouyon, Tarek Hamel

***Abstract*— The paper addresses the control of Vertical Take Off and Landing (VTOL) Underactuated Autonomous Vehicles (UAVs) in hover flight, based on measurements provided by an on-board video camera and rate gyros. The objective is to stabilize the vehicle to the pose associated with a visual image of a planar target. By using the homography matrix computed from the camera measurements of the target, stabilizing feedback laws are derived. Explicit stability conditions on the control parameters are provided. It is shown that very good robustness and performance can be achieved without any apriori information on the visual target (like geometry, or orientation), by a proper tuning of the control parameters. Simulation results confirm the effectiveness of the approach.**

I. Introduction

Unmanned Aerial Vehicles (UAVs) can be used for many surveillance and monitoring applications, both indoor and outdoor. Their effectiveness relies in the first place on the use of onboard sensors that can provide information on the vehicle's *pose* (i.e. position and orientation). In teleoperated modes, the human operator can compensate for the lack of some pose information (like, e.g., the vehicle's position). For fully autonomous control modes, however, information on both position and orientation is necessary. It is well known that pose estimation is a challenging problem for UAVs, and especially for VTOLs (Vertical Take-Off and Landing vehicles). This is due to several reasons, among which, *i)* the absence of sensors that can provide a direct measure of the 3D-orientation (recall that using accelerometers as inclinometers is appropriate only when the vehicle acceleration is small), *ii)* the difficulty to obtain precise and high-rate position measurements via GPS sensors, *iii)* the impossibility to use these sensors in some environments (like, e.g., urban canyons). Thus, while interesting results have been obtained with Inertial Measurement Units (IMUs) [1], or GPS-aided IMUs (see, e.g., [2], [3] for recent results), it is evident that other sensors should be used to improve UAV's effectiveness, especially those providing information about UAV's local environment. One of the most promising alternatives is vision sensors. Cameras provide a rich information about the environment. They have been used extensively for ground robotics applications. Over the last ten years, vision-based control solutions have been extensively developed for aerial vehicles. Regulation of a mechanical system based on visual features as feedback is known as Visual Servo Control [4].

H. de Plinval and P. Mouyon are with ONERA-Toulouse, France, Henry.de_Plinval@onera.fr, Philippe.Mouyon@onera.fr

P. Morin, is with INRIA-Sophia Antipolis, France, Pascal.Morin@inria.fr

T. Hamel is with I3S-CNRS, Nice-Sophia Antipolis, France, thamel@i3s.unice.fr

There are two main approaches in visual servo control [5], [6]: Image-Based Visual Servoing (IBVS), and Position-Based Visual Servoing (PBVS), depending upon whether the controller is designed to directly act on the visual information (IBVS) or whether the visual information is first used in the pose reconstruction (PBVS). The latter has been successfully implemented on a number of aerial vehicles [7], [8], [9], [10]. It requires, however, an accurate geometric model of the visual target along with good calibration of the camera. An IBVS scheme was first presented in [11] where the dynamics of features in image space were formulated in terms of their spherical projections to preserve the dynamic structure of the system and used as direct inputs to the control algorithm. The controller is designed to stabilize the dynamics of the image features, and implicitly solves the underlying task space control problem. This approach does not require an accurate geometric target model or a well calibrated camera, but it leads to complex nonlinear control problems due to the appearance of the image depth as an unknown scale factor into the system dynamics. When the target is planar an alternative approach is the Homography-Based Visual Servoing, originally developed for robot manipulators or more general fully-actuated systems [12], [13], [14]. It consists in a combination of partially reconstructed Euclidean information and 2D image-space information in the control design, and has been shown to have many practical advantages. In particular, the method does not require an accurate model of the target. Homography-Based Visual Servoing for underactuated vehicles has been exploited in different scenarios. In [8] the idea has been exploited to perform a landing manoeuver using a PBVS scheme and in [15] (and subsequently in [16], [17]) in a $2\frac{1}{2}D$ visual servoing formulation. It is important to remark that in these works on homography-based visual servoing of underactuated vehicles, measurements of both the rotation matrix and linear velocities are assumed to be available via complementary sensors.

In this paper we address the problem of controlling VTOL UAVs' hover flight, based on measurements provided by a single camera and rate gyros only. The solution relies on the measure of the homography matrix associated with the camera's observation of a planar target. The assumption of a planar target is not unrealistic when thinking about a landing pad, a planar ground, or a building. There are several challenges associated with this problem. First, since we do not assume any information on the target (like, e.g., size or inclination), the vehicle's pose cannot be extracted from the homography measure. In addition, unlike previous

works on the subject, we do not assume that the vehicle's orientation can be reconstructed (using, e.g., information on the target or additional sensors). Then, we do not have any sensor that provides linear velocity measurements either. Finally, the systems here considered are *underactuated* (i.e. the number of independent force and torque controls is strictly smaller than the number of degrees of freedom). Indeed, most VTOLs encountered in applications belong to this class (e.g., helicopters, X-flyers, ducted fans, etc). The approach builds on a previous result by Benhimane and Malis [13] for the control of robotic manipulators, based on a *kinematic* and *holonomic* model. The fact that *dynamical* models of *underactuated* vehicles are considered here makes the problem significantly harder.

The paper is organized as follows. Section II reviews some technical background and provides a precise description of the addressed problem. In Section III, we propose a new homography-based error vector and specify its relation with the pose error. The main result of the paper, which provides asymptotically stabilizing feedback controllers for VTOL UAVs, is given in Section IV. This is complemented in Section V by a gain-tuning strategy that allows to obtain good performance in a large operating domain. Finally, simulation results are presented in Section VI.

II. Preliminary background

A. Problem statement

The problem addressed in this paper (see Fig. 1 below) corresponds to a typical scenario for UAVs. The vehicle is equipped with a camera. A reference image of a planar target $\mathcal{T}$ is taken at some desired pose (i.e. location), represented by the reference frame $\Re^*$. Based on this reference image and the current image, the objective is to design feedback laws that stabilize the vehicle at the desired pose. In addition to the camera, the vehicle is also equipped with rate gyros. No other sensor is available.

Except for the planarity assumption no other information on the target, like geometry or orientation, is available. In particular, the target's normal is unknown. The distance to the target at the desired pose is also unknown, although a (very rough) lowerbound on this distance is needed to guarantee stability.

Since the systems here considered are *underactuated*, we have to assume that the desired pose is an equilibrium of the vehicle. Otherwise the problem of asymptotic stabilization cannot be solved. For example, in the case of an helicopter, stabilization of a desired pose requires that the rotor thrust direction is vertical at this pose, so as to compensate gravity without inducing lateral motion. This fixes two rotational degrees of freedom.

B. Dynamics of thrust-propelled underactuated vehicles

The approach here proposed applies to the class of underactuated "thrust-propelled" VTOL vehicles [18]. More precisely, we consider rigid bodies with one force control in a body-fixed direction and full torque actuation. Typical examples are given by helicopters, ducted fans, quad-rotors, etc. To comply with the assumption that the reference pose is an equilibrium for the vehicle, it is assumed that the thrust direction at the reference pose is aligned with the vertical basis vector of the reference frame $\Re^*$. The dynamical equations are then given by

$$\left\{\begin{array}{lcl} \dot{p} & = & Rv \\ \dot{R} & = & RS(\omega) \\ m\dot{v} & = & -mS(\omega)v - Tb_3 + m\gamma \\ J\dot{\omega} & = & -S(\omega)J\omega + \Gamma \end{array}\right. \quad (1)$$

with p the position vector of the vehicle's center of mass, expressed in the reference frame, R the rotation matrix from the current frame to the reference frame, v the velocity vector with respect to (w.r.t.) the reference frame expressed in the current frame, ω the angular velocity vector expressed in the current frame, $S(.)$ the matrix-valued function associated with the cross product, i.e. $S(x)y = x \times y\,,\ \forall x, y \in \mathbb{R}^3$, m the mass, T the thrust input, $b_3 = (0, 0, 1)^T$, J the inertia matrix, Γ the torque vector, and $\gamma = gR^T b_3$ the projection of the gravity vector in the current frame with g the gravity constant. Among others, this model describes the dynamics of a helicopter.

Note that the first and second equations of System (1) correspond to the kinematics, while the third and forth account for the dynamics. The objective is to asymptotically stabilize the origin $p = 0, R = I_3, v = 0, \omega = 0$, with I_3 the 3×3 identity matrix, from visual measurements of a reference image $\mathcal{I}^*$ (taken at $\Re^*$) and the current image $\mathcal{I}$ (taken at $\Re$) of the planar target $\mathcal{T}$. Note in particular that neither p nor R are directly measured. Visual measurements only provide a partial and coupled measurement of these quantities (see subsection below). The velocity vector v is not measured either. On the other hand, ω is measured via rate gyros. We review below some well known facts about visual sensors and homography matrices.

C. Visual observation of planar scenes and homography matrices

The following notation relates to the planar scene $\mathcal{T}$ (see Fig. 1 below).

- χ^*, χ are the coordinates of a point of interest $\mathcal{P}$ lying on the planar target, expressed in the reference and current frames respectively.
- n^* is the unit vector defining the normal to the planar object, expressed in the reference frame; d^* is the distance between this plane and the camera optical center. Z^* is the third coordinate of point $\mathcal{P}$ in the reference frame and $c^* = \frac{1}{Z^*}$ its inverse. For simplicity, it is assumed that the z-axis of the body-fixed frame coincides with the camera optical axis.

A useful tool in visual servoing is the so-called homography matrix $\mathbf{H}$ which embeds all information regarding the transformation between two images of the same planar object of interest (see, e.g., [13], [19] for more details). An important feature of this matrix is that it can be estimated from these images without any assumption on the camera

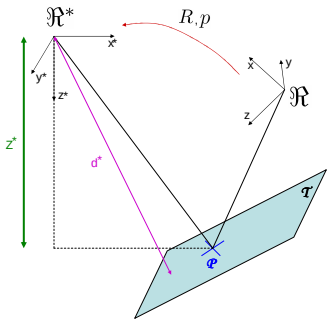

Fig. 1: Problem scheme

pose. It is thus possible to use this matrix to define an error vector that will converge to zero at the desired equilibrium.

Let us first assume that the camera optical center and the vehicle center of mass coincide (this assumption will be discussed latter on). Then, $\mathbf{H}$ is defined as:

$$\mathbf{H} \triangleq K\left(R^T - \frac{1}{d^*}R^T p n^{*T}\right)K^{-1} \tag{2}$$

with K the camera intrinsic parameters matrix. The matrix $\mathbf{H}$ relates the normalized coordinates of a point as seen from the reference and current pose. Indeed, the following relationship holds:

$$\chi = R^T\chi^* - R^T p \tag{3}$$

Defining the pixel coordinates, which embed the camera calibration error, $\mu = K\left(\frac{1}{Z}\chi\right)$ and $\mu^* = K\left(\frac{1}{Z^*}\chi^*\right)$ and noticing that $n^{*T}\chi^* = d^*$, one gets:

$$\begin{aligned}\frac{Z}{Z^*}\mu &= K\left(R^T\frac{\chi^*}{Z^*} - R^T\frac{p}{Z^*}\frac{1}{d^*}n^{*T}\chi^*\right)\\ &= K\left(R^T - \frac{1}{d^*}R^T p n^{*T}\right)K^{-1}\mu^* = \mathbf{H}\mu^*\end{aligned} \tag{4}$$

The scalar $\frac{Z}{Z^*}$ is the unknown ratio of the third coordinates in both frames. This relationship suggests that $\mathbf{H}$ can be estimated only up to an unknown scalar factor. Several algorithms have been proposed for the estimation of the Homography matrix (see, e.g., [13], [19]). Assuming that K is known, we can compute an estimate of the matrix (denoted H_η as opposed to $\mathbf{H}$ which encompasses the calibration error)

$$H_\eta = \eta\left(R^T - \frac{1}{d^*}R^T p n^{*T}\right)$$

with η some scalar factor. One can show (see, e.g., [19, Pg. 135]) that η corresponds to the mean singular value of H_η. Furthermore, an explicit formula for the calculation of η is proposed in [20, App. B]. Therefore, we assume from now on the knowledge of

$$H = R^T - \frac{1}{d^*}R^T p n^{*T} \tag{5}$$

Let us now consider the case when the camera optical center does not coincide with the vehicle center of mass. The camera frame, centered at the optical center, differs from the center of mass frame only by a position offset δ. Let $p_c = p + (R - I)\delta$ denote the position vector of the camera optical center in the reference camera frame. Then, the dynamics of p_c is given by

$$\left\{\begin{array}{lcl}\dot{p}_c &=& Rv_c\\ m\dot{v}_c &=& -mS(\omega)v_c - Tb_3 + m\gamma + Q(\omega) - mS(\delta)\Gamma\end{array}\right.$$

with $v_c = v - S(\delta)\omega$ and Q quadratic in ω. These equations differ from the dynamic equations of p (see (1)) only by the term $Q(\omega) - mS(\delta)\Gamma$. The present approach is based on the design of smooth feedback laws that make the closed-loop system locally exponentially stable (i.e., the state matrix of the linearized closed-loop system is Hurwitz). Since Q is second-order, this term does not affect this stability property. As for $mS(\delta)\Gamma$, this is a first-order term that does not affect the stability for "small enough" values of δ, due to the robustness margin associated with any Hurwitz matrix. We essentially assume in this paper that δ is small enough, so that $mS(\delta)\Gamma$ can be neglected. The general case will be considered in a future work.

The time-derivative of H is easily deduced from (1):

$$\dot{H} = -S(\omega)H - \frac{1}{d^*}vn^{*T}$$

In [13], H was used to define an error vector and an associated feedback law, based on a kinematic control model. More precisely, the following result was shown.

Proposition 2.1: [13, Sec. 4] Let χ^* denote the coordinates of a point $\mathcal{P} \in \mathcal{T}$, expressed in the reference frame $\Re^*$, and $m^* = \frac{1}{Z^*}\chi^* = c^*\chi^*$ the associated normalized coordinates. Let $e \in \mathbb{R}^6$ denote the error vector defined by

$$e = \begin{pmatrix}e_p\\ e_\Theta\end{pmatrix}, \quad e_p = (I - H)m^*, \; e_\Theta = \text{vex}(H^T - H) \tag{6}$$

with vex the function defined by $\text{vex}(S(x)) = x$ for any $x \in \mathbb{R}^3$. Then,

1) $(p, R) \longmapsto e$ defines a local diffeormorphism around $(p, R) = (0, I_3)$. In particular, $e = 0$ if and only if $(p, R) = (0, I_3)$.
2) The kinematic control law

$$v = -\lambda_p e_p, \quad \omega = -\lambda_\Theta e_\Theta \tag{7}$$

with $\lambda_p, \lambda_\Theta > 0$ makes $(p, R) = (0, I_3)$ locally asymptotically stable. △

Remark 2.2: 1) In [13], e_p and e_Θ are defined with an opposite sign, i.e. $e_p = (H - I)m^*$, $e_\Theta = \text{vex}(H - H^T)$. The present choice is better adapted to the definition of v and ω in (1). 2) Note that there is no constraint on m^* except that it must be a projective vector, i.e., $m^*_3 = 1$. △

Extension of Proposition 2.1 to System (1) raises several difficulties. First, the control input is no longer the 6d-vector of velocity variables (v, ω). It is the 4d-vector composed of the force input T and torque vector Γ. Then, the relation between the linear velocity v and the control inputs is

nonlinear and underactuated: there is only one force control variable to control the 3d velocity vector v. Finally, we do not have any measurement of this vector.

III. A NEW ERROR VECTOR

In this section we define a new error which is instrumental in the design of stabilizing feedback laws.

Proposition 3.1: Let $m^* = b_3 = (0,0,1)^T$ and

$$\bar{e} = Me, \quad M = \begin{pmatrix} 2I_3 & S(m^*) \\ -S(m^*) & I_3 \end{pmatrix} \tag{8}$$

with e defined by (6). Let $\Theta = (\phi, \theta, \psi)^T$ denote any parametrization of the rotation matrix R such that $R \approx I_3 + S(\Theta)$ around $R = I_3$ (e.g., Euler angles). Then,

1) $(p, R) \longmapsto \bar{e}$ defines a local diffeormorphism around $(p, R) = (0, I_3)$. In particular, $\bar{e} = 0$ if and only if $(p, R) = (0, I_3)$.
2) In a neighborhood of $(p, R) = (0, I_3)$,

$$\bar{e} = L \begin{pmatrix} p \\ \Theta \end{pmatrix} + O^2(p, \Theta), \quad L = \begin{pmatrix} L_p & 0 \\ L_{p\Theta} & L_\Theta \end{pmatrix} \tag{9}$$

with $L_{p\Theta} = S((\alpha^*, \beta^*, 0)^T)$,

$$L_p = \begin{pmatrix} c^* & 0 & \alpha^* \\ 0 & c^* & \beta^* \\ 0 & 0 & 2c^* \end{pmatrix}, L_\Theta = \begin{pmatrix} 1 & 0 & 0 \\ 0 & 1 & 0 \\ 0 & 0 & 2 \end{pmatrix},$$

α^*, β^* the (unknown) constant scalars defined by $n^* = d^*(\alpha^*, \beta^*, c^*)^T$, and O^2 denoting terms of order two at least. △

The proof, based on elementary first-order approximation of $\bar{e}$, is available upon request to the authors.

Remark 3.2: 1) Since the projective vector m^* is user-defined, the choice $m^* = b_3$ can always be made. As a matter of fact, the present approach can be extended to a general projective vector $m^* = (m_1^*, m_2^*, 1)^T$, by a slight modification of $\bar{e}$. 2) Eq. (9) shows the rationale behind the definition of $\bar{e}$: at first order, components $\bar{e}_1, \bar{e}_2, \bar{e}_3$ contain information on the translation vector p only, while components $\bar{e}_4, \bar{e}_5, \bar{e}_6$ contain decoupled information on the orientation (i.e. L_Θ is diagonal), corrupted by components of the translation vector. Note that L can be viewed as the linear approximation at the origin of the interaction matrix associated with $\bar{e}$. △

Since c^*, α^*, and β^* are unknown, L is not known either. We show below, however, that L contains enough structure for the design of stabilizing control laws.

IV. CONTROL SYNTHESIS

Let $\bar{e}_p \in \mathbb{R}^3$ (resp. $\bar{e}_\Theta \in \mathbb{R}^3$) denote the first (resp. last) three components of $\bar{e}$, i.e. $\bar{e} = (\bar{e}_p^T, \bar{e}_\Theta^T)^T$. The control design relies on a dynamic extension of the state vector defined as follows:

$$\dot{\nu} = -K_7 \nu - \bar{e}_p \tag{10}$$

with K_7 a diagonal gain matrix. The variable ν copes with the lack of measurements of $\dot{\bar{e}}$. The main result of the paper is given next.

Theorem 4.1: Let

$$\begin{cases} T &= m\left(g + k_1 \bar{e}_3 + k_2 \nu_3\right) \\ \Gamma &= -JK_3\left(\omega - \omega^d\right) \end{cases} \tag{11}$$

with

$$\begin{cases} \omega^d &= -\frac{K_4}{g}\left(g\bar{e}_\Theta + b_3 \times \gamma^d\right) \\ \gamma^d &= -K_5 \bar{e}_p - K_6 \nu \end{cases} \tag{12}$$

Then,

1) Given any upper-bound $c_M^* > 0$, there exist diagonal gain matrices $K_i = \mathrm{Diag}(k_i^j)$ $i = 3, \ldots, 7; j = 1, 2, 3$ and scalar gains k_1, k_2, such that the control law (11) makes the equilibrium $(p, R, v, \omega, \nu) = (0, I_3, 0, 0, 0)$ of the closed-loop System (1)-(10) locally exponentially stable for any value of $c^* \in (0, c_M^*]$.
2) If the diagonal gain matrices K_i and scalar gains k_1, k_2 make the closed-loop system locally exponentially stable for $c^* = c_M^*$, then local exponential stability is guaranted for any value of $c^* \in (0, c_M^*]$.

△

The proof is available upon request to the authors.

Let us comment on this result. Since $c^* = 1/Z^*$ and $Z^* \geq d^*$ (recall that $m^* = b_3$), a sufficient condition for $c^* \in (0, c_M^*]$ is that $d^* \geq 1/c_M^*$. Thus, Property 1) ensures that stabilizing control gains can be found given any lower bound on the distance between the reference pose and the observed planar target. This is a very weak requirement from an application point of view. Property 2) is also a very strong result since it implies that in order to find stabilizing control gains for any $c^* \in (0, c_M^*]$, it is sufficient to find stabilizing control gains for $c^* = c_M^*$. This is a much easier task which can be achieved with classical linear control tools. In particular, by using the Routh-Hurwitz criterion, one can show that local exponential stability for $c^* = c_M^*$ is ensured when the following inequalities are satisfied:

$$k_1, k_2, k_i^j > 0\,, \ \forall (i,j) \notin \{(5,3),(6,3)\} \tag{13}$$

$$\begin{cases} k_6^1 < k_5^1 k_7^1 \\ c_M^* a_1^1 a_4^1 (a_4^1 - a_0^1) < a_2^1 D_2^1 \\ c_M^* a_1^1 (a_4^1 - a_0^1)^2 < (a_2^1 - a_0^1 a_3^1) D_2^1 \end{cases} \tag{14}$$

and

$$\begin{cases} k_6^2 < k_5^2 k_7^2 \\ c_M^* a_1^2 a_4^2 (a_4^2 - a_0^2) < a_2^2 D_2^2 \\ c_M^* a_1^2 (a_4^2 - a_0^2)^2 < (a_2^2 - a_0^2 a_3^2) D_2^2 \end{cases} \tag{15}$$

with

$$\begin{gathered} a_0^1 = k_7^1 - \tfrac{k_6^1}{k_5^1}, a_1^1 = k_3^2 k_4^2 k_5^1, a_2^1 = k_3^2 k_4^2 k_7^1, \\ a_3^1 = k_3^2 (k_4^2 + k_7^1), a_4^1 = k_3^2 + k_7^1, D_2^1 = a_4^1 a_3^1 - a_2^1 \end{gathered} \tag{16}$$

and

$$\begin{gathered} a_0^2 = k_7^2 - \tfrac{k_6^2}{k_5^2}, a_1^2 = k_3^1 k_4^1 k_5^2, a_2^2 = k_3^1 k_4^1 k_7^2, \\ a_3^2 = k_3^1 (k_4^1 + k_7^2), a_4^2 = k_3^2 + k_7^2, D_2^2 = a_4^2 a_3^2 - a_2^2 \end{gathered} \tag{17}$$

Let us show the existence of control gains that satisfy these inequalities. First, note that there is no condition on k_5^3 and

k_6^3. This is due to the fact that, by (12), these gains do not affect ω^d. Condition (13) is readily satisfied. Let us consider (14). First, let us remark that this set of conditions involves the control gains $k_3^2, k_4^2, k_5^1, k_6^1$ and k_7^1 only. The gains k_3^2, k_4^2 and k_7^1 can be chosen arbitrarily (under the positivity condition (13)).This fixes the values of a_2^1, a_3^1, a_4^1, and D_2^1. Then, one observes that for $a_0^1 = 0$, the second and third conditions of (14) reduce to $c_M^* a_1^1 (a_4^1)^2 < a_2^1 D_2^1$. Due to the fact that $a_2^1, D_2^1 > 0$, one can choose $a_1^1 > 0$ (via the choice of k_5^1) so that these conditions are satisfied. It is clear by continuity that these conditions are still satisfied for $a_0^1 > 0$ "small enough". This latter condition leads to the choice of k_6^1. Note that $a_0^1 > 0$ guarantees the first condition in (14). Choosing $k_3^1, k_4^1, k_5^2, k_6^2$ and k_7^2 in order to satisfy (15) follows the same procedure.

Let us finally remark that, given a family of control gains, Conditions (13)–(15) allow to determine the maximum value of c_M^* for which exponential stability is obtained.

V. Gain tuning

While stability is a prerequisite for a closed-loop system, performance cannot be neglected in practice. In particular, it matters to ensure good damping properties. This issue is very important here since we have to cope with a large range of the unknown parameter c^*. In this section we propose gain tuning heuristics so as to obtain good performance. These heuristics do not guarantee performance levels, however, we have observed in simulation that they provide good results. Futhermore, after having tuned the gains as proposed, the Barmish theorem [21] can be used to verify performance afterwards. These heuristics are based on the cascade structure of the closed-loop linearized system which allows to address separately the yaw, vertical, and horizontal dynamics. This is similar to the case when full measurement of position, orientation, and velocities is available.

A. Yaw dynamics gain tuning

The characteristic polynomial associated with the (linearized) yaw dynamics is $P(\lambda) = \lambda^2 + k_3^3 \lambda + 2k_3^3 k_4^3$. Thus, any given set of closed-loop poles (λ_1, λ_2) can be assigned by setting

$$k_3^3 = -(\lambda_1 + \lambda_2), \quad k_4^3 = -\frac{\lambda_1 \lambda_2}{2(\lambda_1 + \lambda_2)}$$

B. Vertical dynamics gain tuning

The characteristic polynomial associated with the vertical dynamics is $P(\lambda) = \lambda^2 \left(\lambda + k_7^3\right) + C^* (\lambda + k)$ with $C^* = 2c^* k_1$ and $k = k_7^3 - \frac{k_2}{k_1}$. The following heuristic is proposed:

1) Define the gain k_7^3 and a number $k \neq k_7^3$ knowing that, as c^* grows from 0 to ∞, the closed loop gains will be moving from 0 and $-k_7^3$ to $-k$ and $\frac{k-k_7^3}{2}$.
2) The slowest poles' real parts will start from 0 and head to $\frac{k-k_7^3}{2}$: define the scaling factor k_1 so as to define c_{min}^* for which a given real part is reached. Note that k_2 is then given by: $k_2 = k_1 \left(k_7^3 - k\right)$.
3) Use [21] to assess the performance of the obtained closed-loop system as c^* varies in its allowed range.

Justification: The root locus theory shows that the poles will start from $\left(-k_7^3, 0, 0\right)$ as $c^* = 0$ and head to $-k$ and the two asymptotic directions $\frac{k-k_7^3}{2} \pm j\infty$ as $c^* \to \infty$. One can also verify that, whatever the gains such that $k \neq k_7^3$, there is no root on the imaginary axis.

Numerical example: With $k_1 = 5$, $k_2 = 10$, $k_7^3 = 2.4$, the root locus shows that:

1) $\forall c^* > 0, \Re(\lambda_i) < 0$
2) $\forall c^* \in [0.175; +\infty], -1 \leq \Re(\lambda_i) \leq -0.4$
3) $\forall c^* \in [0.175; 2.34], \xi \geq 0.2$ (ξ is the damping ratio)

C. Horizontal dynamics gain tuning

The horizontal dynamics is composed of two fifth-order linear systems (associated respectively with the roll and pitch dynamics). Since the structure of these systems is the same we only address gain tuning for the first one. The associated characteristic polynomial is:

$$\lambda^2 \left(\lambda + k_7^1\right) \left(\lambda^2 + k_3^2 \lambda + k_3^2 k_4^2\right) + C^* [\lambda + K]$$

where $C = c^* k_3^2 k_4^2 k_5^1, K = k_7^1 - \frac{k_6^1}{k_5^1}$. The following heuristics is proposed:

1) Select k_3^2 and k_4^2 such that the roots of $\lambda^2 + k_3^2 \lambda + k_3^2 k_4^2$ are as fast as possible;
2) Define a much slower dynamics for the "inside system" defined by: $k_3^2 k_4^2 \lambda^2 \left(\lambda + k_7^1\right) + C^* [\lambda + K]$, and select suitable k_5^1, k_6^1, k_7^1 so that for $c^* \in (0; c_M^*]$, all poles are slower than the above defined maximum inside dynamics: see section V.B since the "inside" and vertical dynamics are similar;
3) Use [21] to assess the performance of the obtained closed-loop system as c^* varies in its allowed range.

Justification: From the root locus theory there are poles at 0 (double), $-k_7^1$ and at the roots of $\lambda^2 + k_3^2 \lambda + k_3^2 k_4^2$. The only zero is at $-\left(k_7^1 - \frac{k_6^1}{k_5^1}\right)$ (zero of the inside dynamics). The two poles placed by k_3^2 and k_4^2 will go to infinity as c^* grows. The poles at 0 and $-k_7^1$ will behave similarly to the vertical dynamics for small c^*, since they are close to zero and separated from the first two; for c^* large, two of these poles will escape to infinity with positive real part.

Numerical Example: With gains defined as $k_3^2 = 10, k_4^2 = 12, k_5^1 = 5, k_6^1 = 10, k_7^1 = 2.4$ (inside dynamics being slower than -1, which is must slower than the roots of $\lambda^2 + k_3^2 \lambda + k_3^2 k_4^2$), the characteristic polynom is given by: $\lambda^5 + 12.4\lambda^4 + 144\lambda^3 + 288\lambda^2 + 600c^*\lambda + 240c^*$, which is stable for $c^* \in (0; c_M^*]$ with $c_M^* \approx 4$, and such that the roots real parts $\Re(\lambda) \leq -0.2$ for $c^* \in [c_1^*; c_2^*]$ with $c_1^* \approx 0.2$ and $c_2^* \approx 3.25$.

VI. Simulation results

The proposed approach has been tested via simulations for a dynamical model of an helicopter. This model is defined by (1) with $m = 10kg$ and the coefficients of the inertia

matrix defined by $J_{xx} = 0.3kg.m^2; J_{yy} = 0.8kg.m^2; J_{zz} = 0.9kg.m^2; J_{xy} = 0.1kg.m^2; J_{xz} = 0.2kg.m^2; J_{yz} = 0.1kg.m^2$.

Simulation results reported on Fig. 2–3 have been obtained with initial position offset proportional to the distance: $p_0 = \left(\frac{0.4}{c^*}; -\frac{0.8}{3c^*}; \frac{0.4}{3c^*}\right)^T$. The other initial conditions were null (angles, linear and angular velocity). n^* was chosen as $n^* = (-0.28m; 0.28m; 0.92m)^T$. The control gains in (10)–(11) have been chosen as follows:

$$\begin{array}{l} k_1 = 5,\ k_2 = 10,\ K_3 = \text{Diag}(10, 10, \sqrt{2}) \\ K_4 = \text{Diag}(12, 12, \frac{1}{2\sqrt{2}}),\ K_5 = \text{Diag}(5, 5, 0) \\ K_6 = \text{Diag}(10, 10, 0)\ K_7 = 2.4 I_3 \end{array} \quad (18)$$

This yields, from (14)-(15), the stability upper-bound $c_M^* < 3.99m^{-1}$. Two simulations, obtained with values of $c^* = 0.1m^{-1}$ and $c^* = 2m^{-1}$ are reported. This corresponds to a very large range of distances to the target, with $0.5m \leq Z^* \leq 10m$. Fig. 2–3 show good performance in all this range without using any depth information.

To simulate the effects of measurement noise, simulations have also been conducted with realistic noise levels, i.e. gaussian white noise with standard deviations $0.01rad/s$ for the angular velocity and

$$\begin{pmatrix} 0.0002 & 0.0002 & 0.0454 \\ 0.0002 & 0.0002 & 0.0319 \\ 0 & 0 & 0.0003 \end{pmatrix}$$

for the various elements of the homography matrix. The latter values are based on measurements performed on actual images. In addition, the control values have been passed through a third-order Butterworth filter with $50rad/s$ bandwith. The results are presented on Fig. 4–5. Despite a significant level of noise at the input level, the controller is still able to achieve a fair stabilization around the desired position. Nevertheless, it seems that there is room for improvement in the filtering process.

VII. Conclusion

Stabilizing feedback laws for hover flight control of VTOL UAVs have been proposed based on visual measurements of a planar target and rate gyros measurements. Given any lowerbound on the distance between the target and the vehicle's reference pose, it has been shown that stabilizing feedback laws can be designed without any information on the target. This property could be instrumental in controlling UAVs in unknown environments. Gain tuning strategies have been derived so as to achieve good performance. The approach has been validated in simulation. Extensions of this work include experimental validations on helicopter drones, nonlinear control design in order to possibly extend the stability domain and allow more aggressive manoeuvers, and incorporating accelerometers measurements to better cope with wind gusts.

References

[1] R. Mahony, T. Hamel, and J.-M. Pflimlin, "Non-linear complementary filters on the special orthogonal group," *IEEE Transactions on Automatic Control*, vol. 53, no. 5, pp. 1203–1218, 2008.

[2] P. Martin and E. Salaun, "Design and implementation of a low-cost observer-based attitude and heading reference system," *Control Engineering Practice*, pp. 712–722, 2010.

[3] M.-D. Hua, "Attitude estimation for accelerated vehicles using gps/ins measurements," *Control Engineering Practice*, vol. 18, no. 7, pp. 723–732, 2010.

[4] B. Espiau, "Effect of camera calibration errors on visual servoing in robotics," in *3rd Int. Symp. on Exp. Robot. ser. Lecture Notes in Control and Information Sciences*, vol. 200, no. 1, 1993, pp. 182–192.

[5] F. Chaumette and S.Hutchinson, "Visual servo control, part I: Basic approaches," *IEEE Robotics and Automation Magazine*, vol. 13, no. 4, pp. 82–90, 2006.

[6] ——, "Visual servo control, part II: Advanced approaches," *IEEE Robotics and Automation Magazine*, vol. 14, no. 1, pp. 109–118, 2007.

[7] S. Rathinam, Z. Kim, and R. Sengupta, "Vision based monitoring of locally linear structures using an UAV," *Journal of Infrastructure Systems*, vol. 14, no. 1, pp. 52–63, 2008.

[8] O. Shakernia, Y. Ma, J. Koo, and S. Sastry, "Landing an unmanned air vehicle: Vision based motion estimation and nonlinear control," *Asian Journal of Control*, vol. 1, no. 3, pp. 128–145, 1999.

[9] J. Azinheira and P. Rives, "Image-based visual servoing for vanishing features and ground lines tracking: Application to a UAV," *International Journal of Optomechatronics*, vol. 2, no. 3, pp. 275–295, 2008.

[10] L. Mejias, S. Saripalli, P. Campoy, and G. Sukhatme, "Visual servoing of an autonomous helicopter in urban areas using feature tracking," *In Journal of Field Robotics*, vol. 23, no. 3-4, pp. 185–199, 2006.

[11] T. Hamel and R. Mahony, "Visual servoing of an under-actuated dynamic rigid-body system: An image based approach," *IEEE Transactions on Robotics and Automation*, vol. 18, no. 2, pp. 187–198, 2002.

[12] E. Malis and F. Chaumette, "$2\frac{1}{2}d$ visual servoing with respect to unknown objects through a new estimation scheme of camera displacement," *International Journal of Computer Vision*, vol. 37, no. 1, pp. 79–97, 2000.

[13] S. Benhimane and E. Malis, "Homography-based 2d visual tracking and servoing," *The International Journal of Robotics Research*, pp. 661–676, 2007.

[14] T. Gonalves, J. Azinheira, and P. Rives, "Homography-based visual servoing of an aircraft for automatic approach and landing," in *IEEE Conf. on Robotics and Automation*, 2010, pp. 9–14.

[15] D. Suter, T. Hamel, and R. Mahony, "Visual servo control using homography estimation for the stabilization of an x4-flyer," in *IEEE Conference on Decision and Control*, 2002.

[16] N. Metni, T. Hamel, and F. Derkx, "A uav for bridges inspection: Visual servoing control law with orientation limits," in *5th Symposium on Intelligent Autonomous Vehicles (IAV 04)*, 2004.

[17] V.-K. Chitrakaran, D.-M. Dawson, J. Chen, and F. M., "Vision assisted autonomous landing of an unmanned aerial vehicle," in *IEEE Conference on Decision and Control*, 2005, pp. 1465–1470.

[18] M. Hua, T. Hamel, P. Morin, and C. Samson, "A control approach for thrust-propelled underactuated vehicles and its application to vtol drones," *IEEE Trans. on Automatic Control*, vol. 54, pp. 1837–1853, 2009.

[19] Y. Ma, S. Soatto, J. Kosecka, and S. Sastry, *An Invitation to 3-D Vision: From Images to Geometric Models*. SpringerVerlag, 2003.

[20] E. Malis and M. Vargas, "Deeper understanding of the homography decomposition for vision-based control," INRIA, Tech. Rep. 6303, 2007, available at http://hal.inria.fr/inria-00174036/fr/.

[21] B. Barmish, "A generalization of kharitonov's four-polynomial concept for robust stability problems with linearly dependent coefficient perturbations," *IEEE Trans. on Automatic Control*, vol. 34, pp. 157–165, 1989.

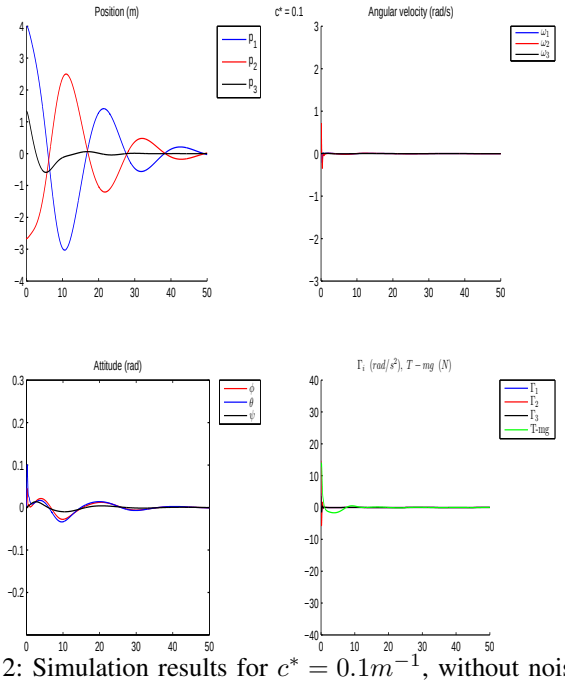

Fig. 2: Simulation results for $c^* = 0.1m^{-1}$, without noise

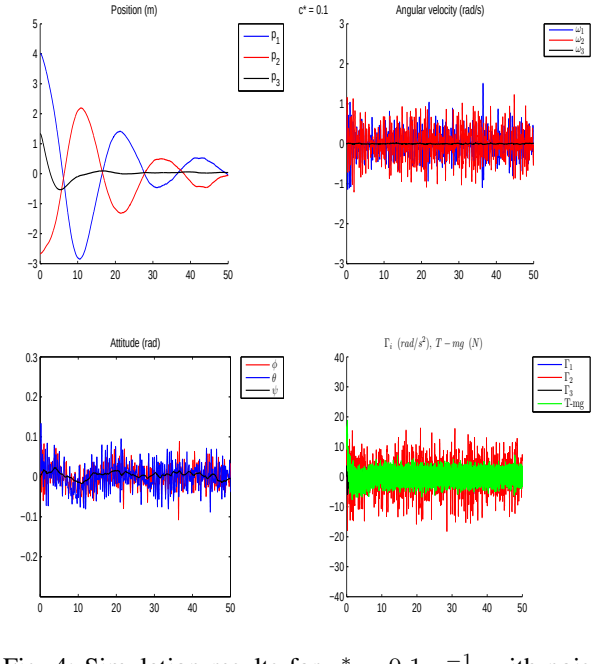

Fig. 4: Simulation results for $c^* = 0.1m^{-1}$, with noise

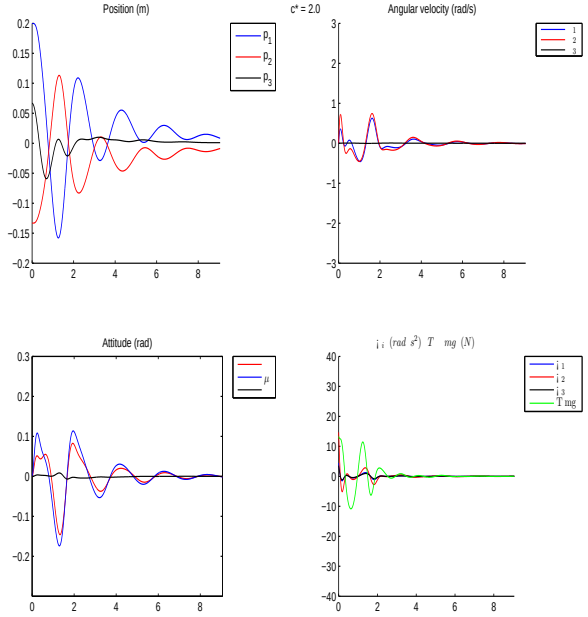

Fig. 3: Simulation results for $c^* = 2m^{-1}$, without noise

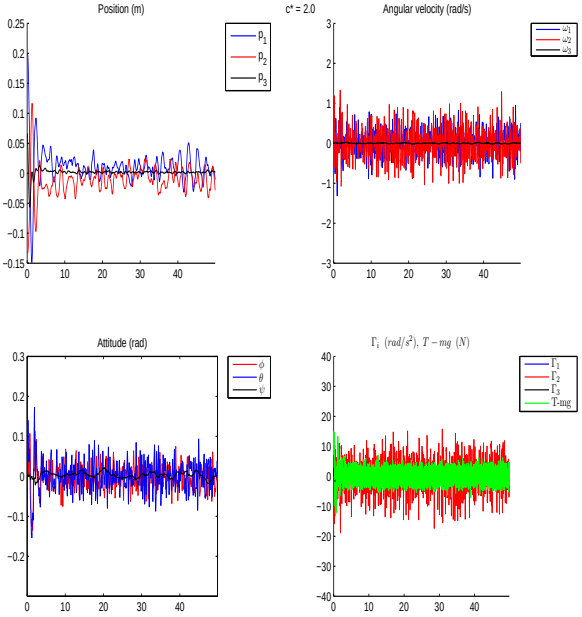

Fig. 5: Simulation results for $c^* = 2m^{-1}$, with noise